

NERVE: Neighbourhood & Entropy-guided Random-walk for training free open-Vocabulary sEgmentation

Kunal Mahatha ✉ Jose Dolz Christian Desrosiers

LIVIA, ÉTS Montréal, Canada

International Laboratory on Learning Systems (ILLS),

McGILL - ETS - MILA - CNRS - Université Paris-Saclay - CentraleSupélec, Canada

✉ kunal.mahatha.1@ens.etsmtl.ca

Abstract

Despite recent advances in Open-Vocabulary Semantic Segmentation (OVSS), existing training-free methods face several limitations: use of computationally expensive affinity refinement strategies, ineffective fusion of transformer attention maps due to equal weighting or reliance on fixed-size Gaussian kernels to reinforce local spatial smoothness, enforcing isotropic neighborhoods. We propose a strong baseline for training-free OVSS termed as NERVE (Neighbourhood & Entropy-guided Random-walk for open-Vocabulary sEgmentation), which uniquely integrates global and fine-grained local information, exploiting the neighbourhood structure from the self-attention layer of a stable diffusion model. We also introduce a stochastic random walk for refining the affinity rather than relying on fixed-size Gaussian kernels for local context. This spatial diffusion process encourages propagation across connected and semantically related areas, enabling it to effectively delineate objects with arbitrary shapes. Whereas most existing approaches treat self-attention maps from different transformer heads or layers equally, our method uses entropy-based uncertainty to select the most relevant maps. Notably, our method does not require any conventional post-processing techniques like Conditional Random Fields (CRF) or Pixel-Adaptive Mask Refinement (PAMR). Experiments are performed on 7 popular semantic segmentation benchmarks, yielding an overall state-of-the-art zero-shot segmentation performance, providing an effective approach to open-vocabulary semantic segmentation.

1. Introduction

Deep learning models have made significant strides in dense image prediction tasks, particularly in semantic segmenta-

tion [29]. However, their reliance on a fixed set of pre-defined classes limits their applicability in numerous real-world scenarios where the categories of interest are often unknown or variable. To address this limitation, open-vocabulary semantic segmentation (OVSS) has recently emerged as a promising alternative [4, 58, 60]. OVSS enables models to recognize and segment novel categories that were not encountered during training, offering greater flexibility and generalization.¹

Most OVSS methods are built on vision-language models, particularly Contrastive Language-Image Pre-training (CLIP) [33], which has demonstrated strong zero-shot performance in visual recognition. These methods generally fall into two broad categories: *training-based* [1, 9, 13, 22, 32, 52, 54–56] and *training-free* [19, 44, 60] approaches. Methods in the first category typically include a fully-supervised (or weakly-supervised) training step, where pixel-wise (or image-wise) annotations from a limited set of categories are used to transfer language–vision relationships from image level to the pixel level. However, these methods still depend on extensive annotations for related categories, and their performance can be influenced by the choice of training dataset used for adaptation [14].

In contrast, training-free methods [2, 3, 10, 16, 19, 21, 28, 38, 44, 47, 60] do not require access to additional data for adaptation, making them suitable for realistic scenarios where large labeled datasets are scarce and novel classes cannot be anticipated. Several methods leverage the visual representations learned by image-level supervised vision transformers (ViTs) such as CLIP. Some approaches modify the self-attention mechanism—for instance, by incorporating query-query or key-key interactions (also known as self-self attention) [3, 19, 21, 44, 60]. Others directly use the value vectors from CLIP as dense features for pixel-

¹Our code is publicly available at: <https://github.com/kunal-mahatha/nerve/>

level classification [60]. An alternative line of work employs additional vision encoders that have been pre-trained using supervised [31], self-supervised [15], or unsupervised [40] learning objectives. More recently, state-of-the-art performance in OVSS has been achieved by harnessing visual features from generative models such as Stable Diffusion [2, 10, 16, 42, 45, 52]. In this paper, we consider the more challenging scenario of training-free OVSS.

Despite the recent advancements in OVSS, current training-free methods for this problem still face notable limitations. First, most of these methods obtain segmentation predictions by combining attention maps from the last ViT layer [11, 14, 19, 20, 42, 44] or from multiple layers with upsampling [18, 41], without taking into account their relative usefulness in the final prediction (e.g., simply averaging the maps). Moreover, methods that rely directly on CLIP’s coarse attention maps typically require an additional segmentation refinement step to address their low spatial resolution [14, 19, 44]. This limitation can be partially mitigated by leveraging the finer-grained attention maps produced by diffusion models [42, 45]. Nevertheless, this comes at a substantial computational cost, as it involves operations over a large, dense similarity matrix that models interactions between all pairs of spatial positions. Additionally, since attention maps do not explicitly capture local spatial relationships, existing approaches may struggle to preserve the contextual integrity of individual objects. To address this, [14] introduced a simple yet effective solution: augmenting attention maps with 2D isotropic Gaussian kernels centered on each patch to increase the attention weight of neighboring regions. While this improves OVSS performance, it assumes that local object context is circular and fixed in size, an assumption that often does not hold in practice. As a result, a separate refinement step is required in post-processing to improve the segmentation.

To address these limitations, we introduce NERVE, a training-free and computationally efficient open-vocabulary semantic segmentation (OVSS) method that exploits neighborhood structure and entropy-guided random walks. NERVE formulates segmentation as a linear stochastic process, where image patches are treated as graph nodes and edge weights determine the transition probabilities between nodes during a random walk. Rather than relying on fixed-size Gaussian kernels to model local object context [14], our method promotes locality within the random walk by assigning higher transition probabilities to neighboring regions. This spatial diffusion process encourages propagation across connected and semantically related areas, enabling the random walk to effectively delineate objects with arbitrary shapes. NERVE also captures pairwise relationships across the entire image efficiently by leveraging the low-rank structure of the self-attention matrix. In contrast to current approaches that explicitly reconstruct the

full attention matrix—resulting in quadratic scaling with the number of patches [42]—our method scales linearly, significantly accelerating the segmentation refinement process. Finally, whereas most existing approaches treat self-attention maps from different transformer heads or layers equally [11, 14, 18–20, 41, 42, 44], our method uses entropy-based uncertainty to select the most relevant maps for the random walk.

Our main contributions can be summarized as follows:

- We propose NERVE, a novel training-free method for open-vocabulary semantic segmentation (OVSS) based on neighborhood- and entropy-guided random walks. A key innovation of NERVE is its ability to efficiently capture *both local and global relationships* within an image, enabling faster and more accurate segmentation. By accounting for the uncertainty across self-attention maps during their combination, NERVE also suppresses noisy relationships that can lead to segmentation errors.
- We motivate our method using a stochastic process that models an infinite-step random walk on a graph, and show how the resulting segmentation can be computed efficiently through either exact or approximate inference.
- We demonstrate the state-of-the-art performance of NERVE through comprehensive experiments conducted on five benchmark datasets and two variants. Additionally, the contribution of each individual component is validated through extensive ablation studies.

2. Related Works

Open-vocabulary semantic segmentation (OVSS) has gained significant attention in recent years [24, 34, 38]. Unlike traditional semantic segmentation, which assumes a fixed set of categories shared between training and testing, OVSS aims to segment objects belonging to arbitrary, potentially unseen categories. Existing methods for this task can be broadly categorized into training-based [7, 27, 35, 51] and training-free approaches [19, 25, 44, 60].

Training-based methods for OVSS can be further categorized into fully-supervised and weakly-supervised approaches. Fully-supervised methods [1, 13, 22, 32, 52, 54, 55] adapt a pre-trained CLIP model for segmentation by leveraging pixel-level annotations from a fixed set of classes, while aiming to retain its generalization to unseen categories. However, the adaptation datasets used in these approaches often exhibit significant class overlap with the test images, potentially inflating performance on unseen classes. In contrast, weakly supervised approaches adapt the CLIP model using only image-level annotations, typically provided as textual descriptions of the categories present in each image [6–8, 26, 46, 50, 57]. Visual–textual alignment is generally achieved through a contrastive loss [50], mirroring CLIP’s original pre-training strategy. This

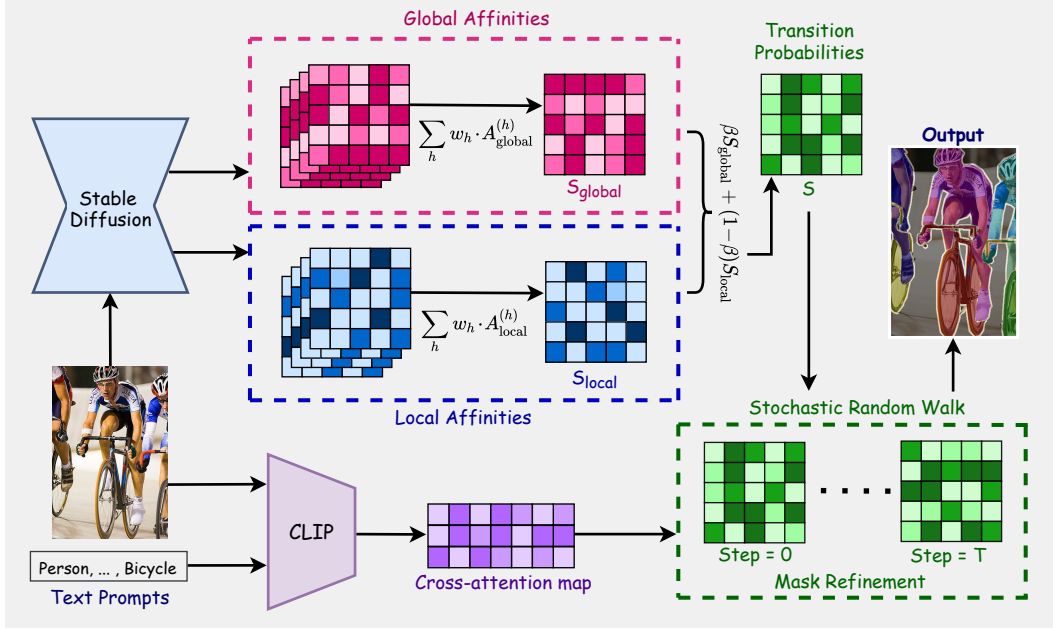


Figure 1. **Overview of our training-free open-vocabulary segmentation pipeline.** Given an image and a set of text prompts, we extract cross-attention maps using CLIP and self-attention maps from a Stable Diffusion encoder. We compute entropy-guided fusion across attention heads h to obtain global (A_{global}) and local (A_{local}) affinities. These are normalized and linearly combined into a final stochastic matrix S , which is used in a truncated stochastic random walk to propagate semantic information and generate refined segmentation masks.

alignment can be further improved by incorporating auxiliary learning techniques, such as online pixel clustering [26] or additional contrastive objectives between features from clean and corrupted image variants [6].

In contrast to training-based approaches, training-free methods [14, 19, 20, 43, 44, 60] repurpose vision-language models like CLIP—originally designed for classification—for segmentation tasks without additional learning. These methods typically rely on CLIP’s embeddings or adapt its attention maps (or their variants) to produce segmentation outputs. For instance, MaskCLIP [60] ignores the final’s layer self-attention maps and instead uses value embeddings of this layer to achieve pixel-level segmentation. Other models like SCLIP [44] and ClearCLIP [19] replace standard self-attention maps with query-to-query or key-to-key attention mechanisms, known as self-self attention. While many methods rely on CLIP’s image encoder to extract visual features, alternative approaches instead utilize diffusion models for this purpose [16, 42, 45, 52]. For instance, DiffSegmenter [45] and iSeg [42] exploit self- and cross-attention maps from a pre-trained Stable Diffusion model [36] to enable open-vocabulary segmentation.

Our work introduces a novel method for OVSS that extends the neighborhood-aware strategy of NACLIP [14] and the iterative refinement approach of iSeg [42] in a efficient framework based on random walks. Unlike NACLIP, which uses fixed-size Gaussian kernels to reinforce attention be-

tween neighboring regions, our approach increases the transition probabilities toward neighboring regions during the random walk. Additionally, we introduce a non-zero stopping probability that encourages locality in the segmentation process. Compared to the refinement strategy of iSeg, which involves computing and manipulating a large dense matrix of size N^2 (with $N = H \times W$, where H and W denote the height and width of the feature map), our NERVE method leverages the low-rank structure of the global attention matrix and the sparsity of the local attention matrix to reduce the computational complexity to be *linear* in N . Finally, related methods often aggregate attention maps from different ViT heads or layers, typically using simple averaging [11, 14, 18–20, 41, 42, 44] or fixed weighting schemes [45]. In contrast, our approach introduces a dynamic weighting mechanism guided by entropy-based uncertainty, enabling more adaptive and informative attention fusion.

3. Methodology

3.1. Random-Walk Model for OVSS

Our training-free OVSS approach, which is summarized in Figure 1, is based on a stochastic process modeling a random-walk on a graph $\mathcal{G} = (\mathcal{V}, \mathcal{E})$, where each node $i \in \mathcal{V}$ corresponds to a spatial token and each edge $(i, j) \in \mathcal{E}$ has a weight $a_{i,j}$ encoding the affinity between nodes i and j . The

main idea is to diffuse the coarse CLIP-based segmentation probabilities using the fine-grained self-attention maps of a diffusion model.

Let $N = |\mathcal{V}|$ be the number of tokens/nodes and as K the number classes in the test set. For each step at an arbitrary node i , the random walk can either *i*) move to a neighbor node with probability $\alpha < 1$, or *ii*) stop the walk and generate a label with probability $1 - \alpha$. In the first case, we select the neighbor node $j \in \mathcal{V}$ with probability

$$s_{i \rightarrow j} := \frac{a_{i,j}}{\sum_{j'} a_{i,j'}}. \quad (1)$$

In the second case, we generate a label y_k with probability $g_{i \rightarrow k}$. Denoting as $S \in \mathbb{R}^{N \times N}$ the row-stochastic node-to-node transition matrix such that $S_{i,j} = s_{i \rightarrow j}$ and $G \in \mathbb{R}^{N \times K}$ the row-stochastic node-to-label generation matrix such that $G_{i,k} = g_{i \rightarrow k}$. The expected probability of generating label y_k in a infinite-length random walk, starting at node i , is given by $[P_\infty]_{i,k}$ where

$$P_\infty := (1 - \alpha) \left(\sum_{t=0}^{\infty} \alpha^t S^t \right) G. \quad (2)$$

with S^t being obtained by multiplying matrix S with itself $t - 1$ times.

While computing this infinite sum directly is impossible, matrix P_∞ can be obtained using a matrix inversion as described in the following theorem.

Theorem 3.1. *The expected label probability matrix P_∞ of Eq. (2) can be computed analytically as*

$$P_\infty = (1 - \alpha) (I - \alpha S)^{-1} G \quad (3)$$

Proof. Consider the partial sum over the L first terms of Eq. (2)

$$\tilde{P}_L := (1 - \alpha) \left(\sum_{t=0}^L \alpha^t S^t \right) G. \quad (4)$$

Pre-multiplying by $(I - \alpha S)$ gives

$$\begin{aligned} (I - \alpha S) \tilde{P}_L &= (1 - \alpha) \left(\sum_{t=0}^L \alpha^t S^t - \sum_{t=1}^{L+1} \alpha^t S^t \right) G \\ &= (1 - \alpha) (I - (\alpha S)^{L+1}) G. \end{aligned} \quad (5)$$

Since $\alpha < 1$, we have that $(\alpha S)^{L+1} \rightarrow 0$ when $L \rightarrow \infty$, hence

$$\begin{aligned} (I - \alpha S) P_\infty &= (1 - \alpha) G \\ P_\infty &= (1 - \alpha) (I - \alpha S)^{-1} G. \end{aligned} \quad (6)$$

□

Nevertheless, inverting a large $(N \times N)$ and potentially dense matrix during training and inference is impractical. In the next sections, we show how the random walk probabilities can be computed efficiently using the low-rankness and sparseness of S .

3.2. Node-to-Node Transition Matrix

Global Affinity Matrix. Building on recent OVSS methods [16, 42, 45], we leverage the attention mechanism of a pre-trained diffusion model to capture global dependencies within the image. Specifically, we use the last two self-attention maps of the Stable Diffusion model [36], which employs a U-Net architecture for its denoising network. Given a feature map with spatial dimensions $H \times W$ and channel dimension D , where each spatial location is treated as a token. The input feature map is first linearly projected into query Q , key K , and value V representations. Attention scores are then calculated as the scaled dot-product between queries and keys, followed by a softmax normalization:

$$A_{\text{self}} := \text{softmax} \left(\frac{QK^\top}{\sqrt{D}} \right), \quad (7)$$

Finally, the output is obtained as $Y = A_{\text{self}} V$. Due to the softmax operation, A_{self} must be constructed explicitly. This leads to a computational complexity that scales quadratically with the number of tokens N , posing a challenge for segmentation tasks that require high-resolution inputs.

To solve this problem, we draw inspiration from linear attention transformers [17] and discard the softmax function to compute our global affinities matrix as

$$[A_{\text{global}}]_{i,j} := \frac{\langle Q_i, K_j \rangle}{\|Q_i\| \cdot \|K_j\|}, \quad (8)$$

with $\langle \cdot, \cdot \rangle$ denoting the dot product.

Local Affinity Matrix. To model local interactions, we define for each token i the set of its immediate spatial neighbors using an 8-connected neighborhood:

$$\begin{aligned} \mathcal{N}(i) &:= \{j : \mathbf{x}_j = \mathbf{x}_i + (dh, dw), \\ &\quad (dh, dw) \in \{-1, 0, 1\}^2 \setminus \{(0, 0)\}\}. \end{aligned}$$

This ensures that each token exchanges information with its spatially adjacent tokens. We then define our *sparse* local affinity matrix as

$$[A_{\text{local}}]_{i,j} := \begin{cases} \epsilon_{\text{self}}, & i = j, \\ \frac{\langle Q_i, K_j \rangle}{\|Q_i\| \cdot \|K_j\|}, & j \in \mathcal{N}(i), \\ 0, & \text{otherwise.} \end{cases} \quad (9)$$

Here, $\epsilon_{\text{self}} > 0$ is a small constant enabling self-transitions in the random walk.

Transition Probability Matrix. To unify the semantic priors captured in the global affinities with the spatial consistency modeled in the local affinities, we apply a linear combination of the two matrices. Toward this goal, we row-normalize them as in Eq. (1) to obtain the stochastic matrices S_{global} and S_{local} . We then compute the transition matrix as

$$S := \beta S_{\text{global}} + (1-\beta)S_{\text{local}}, \quad (10)$$

where $\beta \in [0, 1]$ controls the balance between global and local information. This fused affinity serves as the basis for the final segmentation mask.

3.3. Node-to-Label Generation Matrix

We leverage CLIP’s zero-shot capabilities to define the node-to-label generation matrix G . Specifically, we take the projected query embeddings Q of tokens in the last CLIP layer and the projected key embeddings K of class prompts, and compute the cross-attention map as

$$A_{\text{cross}} := \text{softmax}\left(\frac{QK^\top}{\sqrt{D}}\right). \quad (11)$$

As before, we convert A_{cross} to stochastic matrix G by normalizing its rows.

3.4. Uncertainty-weighted Affinities

The global affinity matrix in Eq. (8) corresponds to a single attention head of the ViT. In our approach, we leverage self-attention maps from 10 different heads: 5 from the final layer and 5 from the penultimate one. A common practice for aggregating these maps is to apply a fixed-weight average, often assigning higher weights to maps from deeper layers [11, 14, 18–20, 41, 42, 44, 45]. However, such fixed strategies fail to capture the image-specific importance of each attention map. To overcome this limitation, we propose a dynamic weighting scheme using entropy-based uncertainty.

Let $A^{(h)} \in \mathbb{R}^{N \times N}$ be the attention map from head h in any layer, and denote as $S^{(h)}$ the stochastic matrix obtained by row-normalizing $A^{(h)}$. A single-step random-walk using $S^{(h)}$ would produce a label probability matrix

$$P_{\text{1-step}}^{(h)} := S^{(h)}G. \quad (12)$$

If $A^{(h)}$ models semantically-relevant relations between different parts of the image, we expect the segmentation to be confident. Hence, we can use the entropy of $P_{\text{1-step}}^{(h)}$ to estimate the usefulness of attention map $A^{(h)}$. Specifically, we compute the entropy of $A^{(h)}$ as

$$\mathcal{H}^{(h)} := -\frac{1}{N} \sum_{i=1}^N \sum_{k=1}^K [P_{\text{1-step}}^{(h)}]_{i,k} \log [P_{\text{1-step}}^{(h)}]_{i,k}. \quad (13)$$

We then use this uncertainty value to obtain a weight w_h measuring the usefulness of $A^{(h)}$:

$$w_h := \frac{\exp(-c \cdot \mathcal{H}^{(h)})}{\sum_{h'} \exp(-c \cdot \mathcal{H}^{(h')})}, \quad (14)$$

where c controls how “peaked” the distribution of weights is. Following this, the uncertainty-weighted affinity matrix is obtained as

$$A_{\text{weighted}} := \sum_{h=1}^H w_h \cdot A^{(h)}. \quad (15)$$

To use this weighted-variant of global affinities, we simply replace S_{global} and S_{local} by their weighted version in Eq. (10).

3.5. Efficient Random-walk Computation

Truncated random-walk. When using a single attention head, matrix S_{global} has the property of being low rank. As described in Supplementary Materials, this enables to compute probabilities P_∞ exactly and efficiently using the Woodbury matrix inversion identity. However, this property vanishes when combining the attention matrices of multiple heads. To overcome this problem, we instead adopt a truncated random-walk approach, where the propagation is performed for a fixed number of steps T :

$$P_L := \frac{1-\alpha}{1-\alpha^{L+1}} \left(\sum_{t=0}^L \alpha^t S^t \right) G \quad (16)$$

Because it truncates the random walk, this strategy may lead to different results than original model of infinite random walk. As shown in the following Theorem, this difference quickly becomes small as we increase the length of the walk.

Theorem 3.1. *Let R_L be the sum of truncated terms in a random walk of length L :*

$$R_L := (1-\alpha) \left(\sum_{t=L+1}^{\infty} \alpha^t S^t \right) G. \quad (17)$$

The $L1$ norm of R_L goes exponentially fast to 0 as we increase the number of steps L .

Proof. Since both S and G are stochastic, we have that $S^t G$

is also stochastic, hence $\|S^t G\|_1 = N$. Therefore,

$$\begin{aligned}
\|R_L\|_1 &= (1-\alpha) \sum_{t=L+1}^{\infty} \alpha^t \|S^t G\|_1 \\
&= N \cdot (1-\alpha) \sum_{t=L+1}^{\infty} \alpha^t \\
&= N \cdot (1-\alpha) \left(\sum_{t=0}^{\infty} \alpha^t - \sum_{t=0}^L \alpha^t \right) \\
&= N \cdot (1-\alpha) \left(\frac{1}{1-\alpha} - \frac{1-\alpha^{L+1}}{1-\alpha} \right) \\
&= N \cdot \alpha^{L+1}.
\end{aligned} \tag{18}$$

□

For $\alpha < 1$, $\|R_L\|_1$ will hence go to zero exponentially fast (geometric decay) as $L \rightarrow \infty$.

Iterative computation. To compute the truncated random-walk efficiently, we employ an iterative strategy where the label probabilities are updated as follows:

$$\tilde{P}_L := (1-\alpha)G + \alpha S \tilde{P}_{L-1}, \quad P_L := \frac{1}{1-\alpha^{L+1}} \tilde{P}_L \tag{19}$$

where \tilde{P}_L is the unnormalized partial sum defined in Eq. (4) and $\tilde{P}_0 = (1-\alpha)G$. Denote as $S^{(h)} := \beta S_{\text{global}}^{(h)} + (1-\beta)S_{\text{local}}^{(h)}$ the transition matrix of diffusion model’s attention head h . Matrix $S_{\text{global}}^{(h)}$ can be expressed in a low rank form as

$$S_{\text{global}}^{(h)} := \tilde{Q}^{(h)}(K^{(h)})^\top \tag{20}$$

where

$$\text{Diag}(Q^{(h)}(K^{(h)})^\top \mathbb{1})^{-1} Q^{(h)} \tag{21}$$

and $\mathbb{1}$ is a vector with all ones. Expanding Eq. (19), we then get

$$\begin{aligned}
\tilde{P}_L &:= (1-\alpha)G + \alpha \sum_{h=1}^H w_h \left(\underbrace{\beta \tilde{Q}^{(h)}((K^{(h)})^\top \tilde{P}_{L-1})}_{\mathcal{O}(N^2 \cdot K \cdot D) + \mathcal{O}(N \cdot K \cdot D^2)} \right. \\
&\quad \left. + (1-\beta) \underbrace{S_{\text{local}}^{(h)} \tilde{P}_{L-1}}_{\mathcal{O}(N \cdot K)} \right).
\end{aligned} \tag{22}$$

For each update step L and every head h , computing the *global* label probabilities using the low rank decomposition has complexity in $\mathcal{O}(N^2 \cdot K \cdot D) + \mathcal{O}(N \cdot K \cdot D^2)$, where N is the number of spatial tokens, K the number of classes and D is the dimension of token features. Likewise, obtaining the *local* probabilities with sparse matrix $S_{\text{local}}^{(h)}$ has a complexity in $\mathcal{O}(N \cdot K)$. For large images, we have that $D \ll N$ thus the overall complexity simplifies to $\mathcal{O}(N^2 \cdot K \cdot D)$. This sharply contrasts with the $\mathcal{O}(N^3 \cdot K)$

complexity of approaches like iSeg [42] that do not leverage the low rank property of attention matrices. The computation of segmentation probabilities is further detailed in the Supplemental Materials.

4. Experiments

4.1. Setup

Datasets. We evaluate NERVE on five standard OVSS benchmarks: PASCAL VOC 2012 (V21) [12], ADE20K-150 (ADE) [59], PASCAL Context (PC60) [30], COCO-Stuff (C-Stf) [5], COCO-Object (C-Obj) [23]. Also, alongside the original benchmarks on these datasets, we follow [42] and evaluate on variants of PASCAL VOC 2012 (V20) and PASCAL Context (PC59) in which the background class is removed from the evaluation.

Baselines. Our method is compared with a relevant set of works in OVSS, including: CLIP [33], MaskCLIP [60], GroupViT [47], GEM [3], SCLIP [44], NACLIP [14], iSeg [42], ClearCLIP [19], ProxyCLIP [20], OVDiff [16], TagCLIP [25], CaR [43], and PixelCLIP [39].

Implementation Details. For our experiments we employ pretrained CLIP-ViT [33], with ViT-L/14 backbone, and Stable Diffusion V2.1 [36]. We set the category descriptions as in SCLIP [44]. Furthermore, the input images are resized to 336×336 . We implemented our approach on a single RTX A6000 with 48G and utilizing less than 10G memory, with the inference being done with batch size of 1 using half precision. Last, we resort to mIoU as the evaluation metric across all experiments.

4.2. Main Results

Comparison to training-free OVSS methods. We report a comprehensive evaluation of NERVE in Tab. 1, where results show that **NERVE consistently outperforms prior approaches without post-processing across all datasets**. On V21, our method achieves an mIoU of 69.4%, surpassing SCLIP (59.1%) and NACLIP (58.9%), and also exceeding the recent diffusion-based iSeg [42] (68.2%). On PC60 and C-Obj, NERVE obtains 37.6% and 43.3% mIoU respectively, outperforming all baselines without post-processing by a substantial margin. Notably, even the best baseline without post-processing, i.e., NACLIP, falls short by over 5% on both PC60 and C-Obj.

Our method also demonstrates strong generalization on benchmarks that exclude background classes, where localization precision is especially critical. On V20, NERVE achieves an mIoU of 90.1%, improving over both GroupViT (79.7%) and ProxyCLIP (83.2%), and approaching CaR (91.0%), a method that requires post-processing. Similarly, on PC59 and C-Stf, NERVE attains 24.0% and 43.4%, substantially outperforming SCLIP (34.2%, 22.4%)

Table 1. **Quantitative evaluation across five datasets and two of their variants.** The first three benchmarks (V21, PC60, and C-Obj) include a background category, whereas the subsequent ones do not. The *Post.* column indicates whether an approach employs post-processing for mask refinement. For explanations of abbreviated benchmark names, refer to Sec. 4.1.

Method		Post.	V21	PC60	C-Obj	V20	ADE	PC59	C-Stf	Avg
CLIP [33]	ICML'21	✗	18.6	7.8	6.5	49.1	3.2	11.2	5.7	13.6
MaskCLIP [60]	ECCV'22	✗	43.4	23.2	20.6	74.9	16.7	26.4	16.7	30.3
GroupViT [50]	CVPR'22	✗	52.3	18.7	27.5	79.7	15.3	23.4	15.3	30.7
CLIP-DIY [47]	WACV'24	✗	59.0	-	30.4	-	-	-	-	-
GEM [3]	CVPR'24	✗	46.2	-	-	-	15.7	32.6	-	-
SCLIP [44]	ECCV'24	✗	59.1	30.4	30.5	80.4	16.1	34.2	22.4	38.2
PixelCLIP [39]	NeurIPS'24	✗	-	-	-	85.9	20.3	37.9	23.6	-
NACLIP [14]	WACV'25	✗	58.9	32.2	33.2	79.9	17.4	35.2	23.3	39.4
iSeg [42]	arXiv'24	✗	68.2	30.9	38.4	-	-	-	-	-
NERVE	Ours	✗	69.7 (↑1.5)	37.7 (↑5.5)	43.3 (↑4.9)	90.1 (↑4.2)	24.0 (↑3.7)	43.4 (↑5.5)	28.8 (↑5.2)	48.1 (↑4.3)
SCLIP [44]	ECCV'24	✓	61.7	31.5	32.1	83.5	17.8	36.1	23.9	40.1
ClearCLIP [19]	ECVA'24	✓	46.1	26.7	30.1	80.0	15.0	29.6	19.9	35.3
ProxyCLIP [20]	ECCV'24	✓	60.6	34.5	39.2	83.2	22.6	37.7	25.6	43.3
OVDiff [16]	CVPR'24	✓	-	-	-	80.9	14.1	32.2	20.3	-
CaR [43]	CVPR'24	✓	67.6	30.5	36.6	91.4	17.7	39.5	-	-
NACLIP [14]	WACV'25	✓	64.1	35.0	36.2	83.0	19.1	38.4	25.7	42.5
NERVE	Ours	✗	69.7 (↑2.1)	37.7 (↑2.7)	43.3 (↑4.1)	90.1 (↓1.3)	24.0 (↑1.4)	43.4 (↑3.9)	28.8 (↑3.1)	48.1 (↑2.3)

and NACLIP (35.2%, 23.3%). Importantly, many of the top-performing methods in recent literature rely on post-processing strategies such as Conditional Random Fields (CRF) or Pixel-Adaptive Mask Refinement (PAMR), as indicated by the (✓) in Tab 1. For example, ProxyCLIP, CaR, and ClearCLIP all incorporate such steps to increase performance. In contrast, NERVE achieves state-of-the-art results *without any* post-processing (✗), relying solely on a single forward pass with our entropy-guided attention fusion and local-global affinity refinement.

Overall, NERVE sets a novel performance benchmark among training-free approaches, with an average mIoU of **48.1%** across all datasets. These results underscore the effectiveness of our design in producing high-quality, spatially consistent segmentations, without relying on additional supervision, or post-hoc refinement.

4.3. Ablations Study

Comparison with Weakly-Supervised Semantic Segmentation (WSSS). To demonstrate the quality of the pseudo-masks generated by NERVE, we compare it against several state-of-the-art WSSS methods. Tab. 2 reports mIoU on the PASCAL VOC 2012 and COCO training sets². Our method yields the highest mIoU on both benchmarks, improving over prior training-free approaches. This underscores the benefit of our entropy-guided fusion and random-walk refinement, which inject spatial coherence without any additional optimization.

²Note that “Training” indicates whether a method requires any per-dataset learning to generate pseudo masks.

Table 2. **Comparison of pseudo-mask generation methods for weakly-supervised semantic segmentation.** We report mIoU on PASCAL VOC 2012 and MS-COCO training sets.

Method		Training	VOC	COCO
MCTformer+ [53]	PAMI'24	✓	68.8	-
ToCo [37]	CVPR'23	✓	72.2	-
WeakTr [61]	CVPR'23	✓	66.2	-
CLIMS [49]	CVPR'22	✓	56.6	-
CLIP-ES [24]	CVPR'23	✗	70.8	39.7
DiffSegmenter [45]	PAMI'25	✗	70.5	-
T2M [48]	NeuroC'24	✗	72.7	43.7
iSeg [42]	arXiv'24	✗	75.2	45.5
NERVE (for iSeg)	Ours	✗	76.2	45.7

Multi-Head Attention Fusion in Stable Diffusion (Tab. 3). To isolate the effect of our entropy-guided fusion mechanism on the multi-head attention maps produced by the Stable Diffusion backbone, we compare three aggregation strategies: (1) *Single*, which selects the best-performing head; (2) *Mean*, which averages all heads uniformly; and (3) *Weighted Mean*, which fuses heads using entropy-based weights that amplify low-entropy (i.e., more focused) heads. As the results show, *Weighted Mean* consistently outperforms both *Single* and *Mean*, achieving 69.4% on VOC (a +2.5 improvement over *Single* and +2.8 over *Mean*), 37.6% on Context (+1.0 over *Single* and +1.1 over *Mean*), and 43.3% on Object (+1.3 over *Single* and +1.6 over *Mean*). These gains confirm that entropy-guided weighting effectively suppresses noisy or diffuse heads while emphasizing the most informative ones,



Figure 2. **Impact of random-walk iteration count on segmentation mIoU.** Evolution of mIoU on PASCAL VOC, VOC21, and PC59 as a function of the number of stochastic random-walk refinement steps, demonstrating rapid gains up to 20 iterations and saturation thereafter.

yielding more accurate segmentation masks. Consequently, we adopt *Weighted Mean* as our default fusion strategy in all subsequent experiments.

Table 3. **Comparison of multi-head attention fusion strategies in Stable Diffusion.** “Single” selects the best head, “Mean” averages all heads, and “Weighted Mean” uses entropy-based head weighting.

Type	VOC	Context	Object
Single	67.2	36.6	42.0
Mean	66.9	36.5	41.7
Weighted Mean	69.7	37.6	43.3

Affinity Map Variants (Table 4). We evaluate three types of affinity maps: (1) *Global*, derived directly from raw self-attention affinity; (2) *Local*, built via cosine similarity between neighboring tokens; and (3) *Global+Local+RW*, which refines the combined affinity through a stochastic random-walk (RW). As shown in Table 4, the *Global+Local+RW* configuration consistently outperforms others (e.g., achieving 69.7% on VOC). This confirms that integrating global semantic cues, local spatial coherence, and RW-based refinement significantly boosts segmentation accuracy.

Effect of Random-Walk Iteration Count on Segmentation mIoU (Fig. 2). As shown in Fig. 2, segmentation performance steadily improves as the number of random-walk iterations increases. Starting from the 0-step baseline (89.2% in VOC, 63.3% in VOC21, and 40.0% in PC59), 5 random-walk iterations raise mIoU to 89.7%, 67.5%, and 42.5%, respectively. At 10 steps, performance



Figure 3. **Progressive segmentation refinement via Stochastic Random Walk.** For each image, we visualize the effect of increasing random walk steps on the segmentation map. Regions of interest are highlighted with colored boxes. Our method produces increasingly accurate and coherent segmentations over time, illustrating strong local-global propagation.

Table 4. **Ablation on different affinity maps.** Global represents the affinity map coming directly from the self attention layer. Local represents the affinity constructed using cosine similarity explained above, whereas RW represents the stochastic random walk process used for mask refinement.

Type	VOC	Context	Object
Global	63.3	35.0	39.8
Local	58.7	34.5	37.6
Global + Local + RW	69.7	37.6	43.4

increases to 89.9%, 68.7%, and 43.1%. Refinement with 40 iterations yields mIoU values of 90.1%, 69.4%, and 43.4% on the three benchmarks. Beyond 40 steps, results plateau, indicating convergence.

4.4. Qualitative Results

To explore the effect of stochastic random walk, we visualize its progression across different steps in Fig. 3. We highlight and zoom in on a small region (marked by colored bounding boxes) to show the segmentation output at steps: 1, 5, 10, 20, 40. We notice that in the early steps (i.e., Steps 1 to 5), it can propagate the semantic structure to its neighbors. As the steps increase, the segmentation boundaries become sharper. Notably, at Step 40, the segmentation boundaries are well aligned with visual cues. This improvement is evident across various objects and scenes. In the first row, the green mask of the cow becomes more complete as the walk progresses, while in the second row, even finer details on the bus are filled in by the yellow mask despite the cluttered background. Finally, in the last row, the pink mask on the dog’s face noticeably becomes more accurate

to the edges. This demonstrates our method’s robustness across all objects and contexts.

5. Conclusion

Utilizing the zero-capability of CLIP and Stable Diffusion in the OVSS domain, this method achieves a significant performance boost and is emerging as an alternative to closed-set supervised training. Our method **NERVE** has three main components: an entropy-based weighted mean of the global and local affinity map, and a stochastic random walk for affinity map refinement. The local-global affinity aims to reduce the irrelevant global information typically generated by the self-attention map, and the stochastic random walk, in combination, pays more attention to the features of the segmented class, making this method preferable for semantic segmentation tasks. Extensive experiments on the well-known and recent OVSS benchmark show the superiority of the existing OVSS methods. The empirical observations highlight that our approach yields state-of-the-art performance on post-processing-free methods, and even with methods that require post-processing, our method outperforms 6 out of 7 benchmarks. **NERVE**, does not require access to any labelled or unlabelled data, which makes it suitable for real-world applications.

References

- [1] Luca Barsellotti, Roberto Amoroso, Lorenzo Baraldi, and Rita Cucchiara. Enhancing open-vocabulary semantic segmentation with prototype retrieval. In *International Conference on Image Analysis and Processing*, pages 196–208. Springer, 2023. 1, 2
- [2] Luca Barsellotti, Roberto Amoroso, Lorenzo Baraldi, and Rita Cucchiara. FOSSIL: Free open-vocabulary semantic segmentation through synthetic references retrieval. In *Proceedings of the IEEE/CVF Winter Conference on Applications of Computer Vision*, pages 1464–1473, 2024. 1, 2
- [3] Walid Bousselham, Felix Petersen, Vittorio Ferrari, and Hilde Kuehne. Grounding everything: Emerging localization properties in vision-language transformers. In *Proceedings of the IEEE/CVF Conference on Computer Vision and Pattern Recognition*, pages 3828–3837, 2024. 1, 6, 7
- [4] Maxime Bucher, Tuan-Hung Vu, Matthieu Cord, and Patrick Pérez. Zero-shot semantic segmentation. *Advances in Neural Information Processing Systems*, 32, 2019. 1
- [5] Holger Caesar, Jasper Uijlings, and Vittorio Ferrari. COCO-Stuff: Thing and stuff classes in context. In *Proceedings of the IEEE/CVF Conference on Computer Vision and Pattern Recognition*, 2018. 6
- [6] Kaixin Cai, Pengzhen Ren, Yi Zhu, Hang Xu, Jianzhuang Liu, Changlin Li, Guangrun Wang, and Xiaodan Liang. MixReorg: Cross-modal mixed patch reorganization is a good mask learner for open-world semantic segmentation. In *Proceedings of the IEEE/CVF International Conference on Computer Vision*, pages 1196–1205, 2023. 2, 3
- [7] Junbum Cha, Jonghwan Mun, and Byungseok Roh. Learning to generate text-grounded mask for open-world semantic segmentation from only image-text pairs. In *Proceedings of the IEEE/CVF Conference on Computer Vision and Pattern Recognition*, pages 11165–11174, 2023. 2
- [8] Jun Chen, Deyao Zhu, Guocheng Qian, Bernard Ghanem, Zhicheng Yan, Chenchen Zhu, Fanyi Xiao, Sean Chang Culatana, and Mohamed Elhoseiny. Exploring open-vocabulary semantic segmentation from CLIP vision encoder distillation only. In *Proceedings of the IEEE/CVF International Conference on Computer Vision*, pages 699–710, 2023. 2
- [9] Seokju Cho, Heeseong Shin, Sunghwan Hong, Anurag Arnab, Paul Hongsuck Seo, and Seungryong Kim. CAT-Seg: Cost aggregation for open-vocabulary semantic segmentation. In *Proceedings of the IEEE/CVF Conference on Computer Vision and Pattern Recognition*, pages 4113–4123, 2024. 1
- [10] Barbara Toniella Corradini, Mustafa Shukor, Paul Couairon, Guillaume Couairon, Franco Scarselli, and Matthieu Cord. FreeSeg-Diff: Training-free open-vocabulary segmentation with diffusion models. *arXiv preprint arXiv:2403.20105*, 2024. 1, 2
- [11] Zheng Ding, Jieke Wang, and Zhuowen Tu. Open-vocabulary universal image segmentation with MaskCLIP. In *Proceedings of the 40th International Conference on Machine Learning*, pages 8090–8102, 2023. 2, 3, 5
- [12] Mark Everingham, SM Ali Eslami, Luc Van Gool, Christopher KI Williams, John Winn, and Andrew Zisserman. The pascal visual object classes challenge: A retrospective. *International Journal of Computer Vision*, 2015. 6
- [13] Golnaz Ghiasi, Xiuye Gu, Yin Cui, and Tsung-Yi Lin. Scaling open-vocabulary image segmentation with image-level labels. In *European conference on computer vision*, pages 540–557. Springer, 2022. 1, 2
- [14] Sina Hajimiri, Ismail Ben Ayed, and Jose Dolz. Pay Attention to Your Neighbours: Training-free open-vocabulary semantic segmentation. *Proceedings of the Winter Conference on Applications of Computer Vision (WACV)*, 2024. 1, 2, 3, 5, 6, 7
- [15] Kaiming He, Haoqi Fan, Yuxin Wu, Saining Xie, and Ross Girshick. Momentum contrast for unsupervised visual representation learning. In *Proceedings of the IEEE/CVF conference on computer vision and pattern recognition*, pages 9729–9738, 2020. 2
- [16] Laurynas Karazija, Iro Laina, Andrea Vedaldi, and Christian Rupprecht. Diffusion models for zero-shot open-vocabulary segmentation. *arXiv preprint arXiv:2306.09316*, 2023. 1, 2, 3, 4, 6, 7
- [17] Angelos Katharopoulos, Apoorv Vyas, Nikolaos Pappas, and François Fleuret. Transformers are RNNs: Fast autoregressive transformers with linear attention. In *International conference on machine learning*, pages 5156–5165. PMLR, 2020. 4
- [18] Aliasghar Khani, Saeid Asgari Taghanaki, Aditya Sanghi, Ali Mahdavi Amiri, and Ghassan Hamarneh. SLiMe: Segment like me. *arXiv preprint arXiv:2309.03179*, 2023. 2, 3, 5

- [19] Mengcheng Lan, Chaofeng Chen, Yiping Ke, Xinjiang Wang, Litong Feng, and Wayne Zhang. ClearCLIP: Decomposing CLIP representations for dense vision-language inference. In *European Conference on Computer Vision*, 2024. 1, 2, 3, 6, 7
- [20] Mengcheng Lan, Chaofeng Chen, Yiping Ke, Xinjiang Wang, Litong Feng, and Wayne Zhang. ProxyCLIP: Proxy attention improves CLIP for open-vocabulary segmentation. In *European Conference on Computer Vision*, 2024. 2, 3, 5, 6, 7
- [21] Yi Li, Hualiang Wang, Yiqun Duan, and Xiaomeng Li. CLIP surgery for better explainability with enhancement in open-vocabulary tasks. *arXiv e-prints*, pages arXiv-2304, 2023. 1
- [22] Feng Liang, Bichen Wu, Xiaoliang Dai, Kunpeng Li, Yinan Zhao, Hang Zhang, Peizhao Zhang, Peter Vajda, and Diana Marculescu. Open-vocabulary semantic segmentation with mask-adapted CLIP. In *Proceedings of the IEEE/CVF conference on computer vision and pattern recognition*, pages 7061–7070, 2023. 1, 2
- [23] Tsung-Yi Lin, Michael Maire, Serge Belongie, James Hays, Pietro Perona, Deva Ramanan, Piotr Dollár, and C Lawrence Zitnick. Microsoft COCO: Common objects in context. In *European Conference on Computer Vision*, pages 740–755. Springer, 2014. 6
- [24] Yuqi Lin, Minghao Chen, Wenxiao Wang, Boxi Wu, Ke Li, Binbin Lin, Haifeng Liu, and Xiaofei He. CLIP is also an efficient segmenter: A text-driven approach for weakly supervised semantic segmentation. In *Proceedings of the IEEE/CVF Conference on Computer Vision and Pattern Recognition (CVPR)*, pages 15305–15314, 2023. 2, 7
- [25] Yuqi Lin, Minghao Chen, Kaipeng Zhang, Hengjia Li, Mingming Li, Zheng Yang, Dongqin Lv, Binbin Lin, Haifeng Liu, and Deng Cai. TagCLIP: A local-to-global framework to enhance open-vocabulary multi-label classification of CLIP without training. In *Proceedings of the AAAI Conference on Artificial Intelligence*, pages 3513–3521, 2024. 2, 6
- [26] Quande Liu, Youpeng Wen, Jianhua Han, Chunjing Xu, Hang Xu, and Xiaodan Liang. Open-world semantic segmentation via contrasting and clustering vision-language embedding. In *European Conference on Computer Vision*, pages 275–292. Springer, 2022. 2, 3
- [27] Huaishao Luo, Junwei Bao, Youzheng Wu, Xiaodong He, and Tianrui Li. SegCLIP: Patch aggregation with learnable centers for open-vocabulary semantic segmentation. In *International Conference on Machine Learning*, pages 23033–23044. PMLR, 2023. 2
- [28] Jiayun Luo, Siddhesh Khandelwal, Leonid Sigal, and Boyang Li. Emergent open-vocabulary semantic segmentation from off-the-shelf vision-language models. In *Proceedings of the IEEE/CVF Conference on Computer Vision and Pattern Recognition*, pages 4029–4040, 2024. 1
- [29] Shervin Minaee, Yuri Boykov, Fatih Porikli, Antonio Plaza, Nasser Kehtarnavaz, and Demetri Terzopoulos. Image segmentation using deep learning: A survey. *IEEE transactions on pattern analysis and machine intelligence*, 44(7):3523–3542, 2021. 1
- [30] Roozbeh Mottaghi, Xianjie Chen, Xiaobai Liu, Nam-Gyu Cho, Seong-Whan Lee, Sanja Fidler, Raquel Urtasun, and Alan Yuille. The role of context for object detection and semantic segmentation in the wild. In *Proceedings of the IEEE/CVF Conference on Computer Vision and Pattern Recognition*, 2014. 6
- [31] Muhammad Muzammal Naseer, Kanchana Ranasinghe, Salman H Khan, Munawar Hayat, Fahad Shahbaz Khan, and Ming-Hsuan Yang. Intriguing properties of vision transformers. *Advances in Neural Information Processing Systems*, 34: 23296–23308, 2021. 2
- [32] Jie Qin, Jie Wu, Pengxiang Yan, Ming Li, Ren Yuxi, Xuefeng Xiao, Yitong Wang, Rui Wang, Shilei Wen, Xin Pan, et al. FreeSeg: Unified, universal and open-vocabulary image segmentation. In *Proceedings of the IEEE/CVF Conference on Computer Vision and Pattern Recognition*, pages 19446–19455, 2023. 1, 2
- [33] Alec Radford, Jong Wook Kim, Chris Hallacy, Aditya Ramesh, Gabriel Goh, Sandhini Agarwal, Girish Sastry, Amanda Askell, Pamela Mishkin, Jack Clark, et al. Learning transferable visual models from natural language supervision. In *International Conference on Machine Learning*, pages 8748–8763, 2021. 1, 6, 7
- [34] Kanchana Ranasinghe, Brandon McKinzie, Sachin Ravi, Yinfei Yang, Alexander Toshev, and Jonathon Shlens. Perceptual grouping in contrastive vision-language models. In *Proceedings of the IEEE/CVF International Conference on Computer Vision*, pages 5571–5584, 2023. 2
- [35] Pengzhen Ren, Changlin Li, Hang Xu, Yi Zhu, Guangrun Wang, Jianzhuang Liu, Xiaojun Chang, and Xiaodan Liang. ViewCo: Discovering text-supervised segmentation masks via multi-view semantic consistency. *arXiv preprint arXiv:2302.10307*, 2023. 2
- [36] Robin Rombach, Andreas Blattmann, Dominik Lorenz, Patrick Esser, and Björn Ommer. High-resolution image synthesis with latent diffusion models. In *Proceedings of the IEEE/CVF conference on computer vision and pattern recognition*, pages 10684–10695, 2022. 3, 4, 6
- [37] Lixiang Ru, Heliang Zheng, Yibing Zhan, and Bo Du. Token contrast for weakly-supervised semantic segmentation. In *CVPR*, 2023. 7
- [38] Gyungin Shin, Weidi Xie, and Samuel Albanie. ReCo: Retrieve and co-segment for zero-shot transfer. *Advances in Neural Information Processing Systems*, 35:33754–33767, 2022. 1, 2
- [39] Heeseong Shin, Chaehyun Kim, Sunghwan Hong, Seokju Cho, Anurag Arnab, Paul Hongsuck Seo, and Seungryong Kim. Towards open-vocabulary semantic segmentation without semantic labels. *arXiv preprint arXiv:2409.19846*, 2024. 6, 7
- [40] Oriane Siméoni, Chloé Sekkat, Gilles Puy, Antonín Vobecký, Éloi Zablocki, and Patrick Pérez. Unsupervised object localization: Observing the background to discover objects. In *Proceedings of the IEEE/CVF conference on computer vision and pattern recognition*, pages 3176–3186, 2023. 2
- [41] Lin Sun, Jiale Cao, Jin Xie, Xiaoheng Jiang, and Yanwei Pang. CLIPer: Hierarchically improving spatial represen-

- tation of CLIP for open-vocabulary semantic segmentation. *arXiv preprint arXiv:2411.13836*, 2024. 2, 3, 5
- [42] Lin Sun, Jiale Cao, Jin Xie, Fahad Shahbaz Khan, and Yanwei Pang. iSeg: An iterative refinement-based framework for training-free segmentation. *arXiv preprint arXiv:2409.03209*, 2024. 2, 3, 4, 5, 6, 7
- [43] Shuyang Sun, Runjia Li, Philip Torr, Xiuye Gu, and Siyang Li. CLIP as RNN: Segment countless visual concepts without training endeavor. In *IEEE/CVF Conference on Computer Vision and Pattern Recognition*, pages 13171–13182, 2024. 3, 6, 7
- [44] Feng Wang, Jieru Mei, and Alan Yuille. SCLIP: Rethinking self-attention for dense vision-language inference. *European Conference on Computer Vision*, 2024. 1, 2, 3, 5, 6, 7
- [45] Jinglong Wang, Xiawei Li, Jing Zhang, Qingyuan Xu, Qin Zhou, Qian Yu, Lu Sheng, and Dong Xu. Diffusion model is secretly a training-free open vocabulary semantic segmenter. *IEEE Transactions on Image Processing*, 34:1895–1907, 2025. 2, 3, 4, 5, 7
- [46] Size Wu, Wenwei Zhang, Lumin Xu, Sheng Jin, Xiangtai Li, Wentao Liu, and Chen Change Loy. CLIPself: Vision transformer distills itself for open-vocabulary dense prediction. *arXiv preprint arXiv:2310.01403*, 2023. 2
- [47] Monika Wysoczańska, Michaël Ramamonjisoa, Tomasz Trzcinski, and Oriane Siméoni. CLIP-DIY: CLIP dense inference yields open-vocabulary semantic segmentation for-free. In *Proceedings of the IEEE/CVF Winter Conference on Applications of Computer Vision*, pages 1403–1413, 2024. 1, 6, 7
- [48] Changming Xiao, Qi Yang, Feng Zhou, and Changshui Zhang. From text to mask: Localizing entities using the attention of text-to-image diffusion models. *Neurocomputing*, 610:128437, 2024. 7
- [49] Jinheng Xie, Xianxu Hou, Kai Ye, and Linlin Shen. Clims: Cross language image matching for weakly supervised semantic segmentation. In *Proceedings of the IEEE/CVF Conference on Computer Vision and Pattern Recognition (CVPR)*, pages 4483–4492, 2022. 7
- [50] Jiarui Xu, Shalini De Mello, Sifei Liu, Wonmin Byeon, Thomas Breuel, Jan Kautz, and Xiaolong Wang. GroupViT: Semantic segmentation emerges from text supervision. In *Proceedings of the IEEE/CVF Conference on Computer Vision and Pattern Recognition*, 2022. 2, 7
- [51] Jilan Xu, Junlin Hou, Yuejie Zhang, Rui Feng, Yi Wang, Yu Qiao, and Weidi Xie. Learning open-vocabulary semantic segmentation models from natural language supervision. In *Proceedings of the IEEE/CVF conference on computer vision and pattern recognition*, pages 2935–2944, 2023. 2
- [52] Jiarui Xu, Sifei Liu, Arash Vahdat, Wonmin Byeon, Xiaolong Wang, and Shalini De Mello. Open-vocabulary panoptic segmentation with text-to-image diffusion models. In *Proceedings of the IEEE/CVF conference on computer vision and pattern recognition*, pages 2955–2966, 2023. 1, 2, 3
- [53] Lian Xu, Mohammed Bennamoun, Farid Boussaid, Hamid Laga, Wanli Ouyang, and Dan Xu. MCTformer+: Multi-class token transformer for weakly supervised semantic segmentation. *IEEE Transactions on Pattern Analysis and Machine Intelligence*, 46(12):8380–8395, 2024. 7
- [54] Mengde Xu, Zheng Zhang, Fangyun Wei, Yutong Lin, Yue Cao, Han Hu, and Xiang Bai. A simple baseline for open-vocabulary semantic segmentation with pre-trained vision-language model. In *European Conference on Computer Vision*, pages 736–753. Springer, 2022. 1, 2
- [55] Mengde Xu, Zheng Zhang, Fangyun Wei, Han Hu, and Xiang Bai. Side adapter network for open-vocabulary semantic segmentation. In *Proceedings of the IEEE/CVF conference on computer vision and pattern recognition*, pages 2945–2954, 2023. 2
- [56] Qihang Yu, Ju He, Xueqing Deng, Xiaohui Shen, and Liang-Chieh Chen. Convolutions die hard: Open-vocabulary segmentation with single frozen convolutional CLIP. *Advances in Neural Information Processing Systems*, 36:32215–32234, 2023. 1
- [57] Fei Zhang, Tianfei Zhou, Boyang Li, Hao He, Chaofan Ma, Tianjiao Zhang, Jiangchao Yao, Ya Zhang, and Yanfeng Wang. Uncovering prototypical knowledge for weakly open-vocabulary semantic segmentation. *Advances in Neural Information Processing Systems*, 36:73652–73665, 2023. 2
- [58] Hang Zhao, Xavier Puig, Bolei Zhou, Sanja Fidler, and Antonio Torralba. Open vocabulary scene parsing. In *Proceedings of the IEEE International Conference on Computer Vision*, pages 2002–2010, 2017. 1
- [59] Bolei Zhou, Hang Zhao, Xavier Puig, Tete Xiao, Sanja Fidler, Adela Barriuso, and Antonio Torralba. Semantic understanding of scenes through the ADE20k dataset. *International Journal of Computer Vision*, 2019. 6
- [60] Chong Zhou, Chen Change Loy, and Bo Dai. Extract free dense labels from CLIP. In *European Conference on Computer Vision*, 2022. 1, 2, 3, 6, 7
- [61] Lianghui Zhu, Yingyue Li, Jiemin Fang, Yan Liu, Hao Xin, Wenyu Liu, and Xinggang Wang. Weaktr: Exploring plain vision transformer for weakly-supervised semantic segmentation. *arxiv:2304.01184*, 2023. 7